

1
2
3
4
5
6
7
8
9
10
11
12
13
14
15
16
17
18
19
20
21
22
23
24
25
26
27
28
29

Cauliflower fractal forms arise from perturbations of floral gene networks

Eugenio Azpeitia^{1,‡}, Gabrielle Tichtinsky², Marie Le Masson², Antonio Serrano-Mislata³, Jérémy Lucas², Veronica Gregis⁴, Carlos Gimenez³, Nathanaël Prunet⁵, Etienne Farcot⁶, Martin M.Kater⁴, Desmond Bradley⁷, Francisco Madueño³, Christophe Godin^{1,*}, Francois Parcy^{2,*}

1: Laboratoire de Reproduction et Développement des Plantes, Univ. Lyon, ENS de Lyon, UCB Lyon 1, CNRS, INRAE, Inria, 46 allée d'Italie, F-69364, Lyon, France

2: Laboratoire Physiologie Cellulaire et Végétale, Univ. Grenoble Alpes, CNRS, CEA, INRAE, IRIG-DBSCI-LPCV, 17 avenue des martyrs, F-38054, Grenoble, France

3: Instituto de Biología Molecular y Celular de Plantas (IBMCP), Consejo Superior de Investigaciones Científicas (CSIC) - Universidad Politécnica de Valencia (UPV), 46022 Valencia, Spain.

4: Dipartimento di Bioscienze, Università degli Studi di Milano, Via Celoria 26, 20133 Milan, Italy

5: Division of Biology and Biological Engineering, California Institute of Technology, 1200 E. California Blvd., Pasadena, CA 91125, USA and Department of Molecular, Cell and Developmental Biology, University of California, Los Angeles, 610 Charles E. Young dr. S., Los Angeles, CA 90095, USA

6: School of Mathematical Sciences, University of Nottingham, NG7 2RD, United Kingdom.

7: Department of Cell and Developmental Biology, John Innes Centre, NR4 7UH Norwich NR4 7UH, United Kingdom.

‡: Present address, Centro de Ciencias Matemáticas, Universidad Nacional Autónoma de México, Morelia, México

*: Co-corresponding authors.

30 One Sentence Summary

31

32 The molecular making of cauliflowers

33

34 Abstract

35

36 Throughout development, plant meristems regularly produce organs in defined spiral, opposite or
37 whorl patterns, called phyllotaxis. Cauliflowers present an unusual phyllotaxis with a multitude
38 of spirals nested over a wide range of scales. How such a fractal self-similar organization
39 emerges from developmental mechanisms has remained elusive. Combining experimental
40 analyses in *Arabidopsis thaliana* cauliflower-like mutant with modeling, we found that curd self-
41 similarity arises because the meristems fail to form flowers but keep the “memory” of their
42 transient passage in a floral state. Additional mutations affecting meristem growth can induce the
43 production of conical phyllotactic structures reminiscent of the conspicuous fractal Romanesco
44 shape. This study reveals how fractal-like forms may emerge from the combination of key,
45 defined perturbations of floral developmental programs and growth dynamics.

46

47 Main Text

48

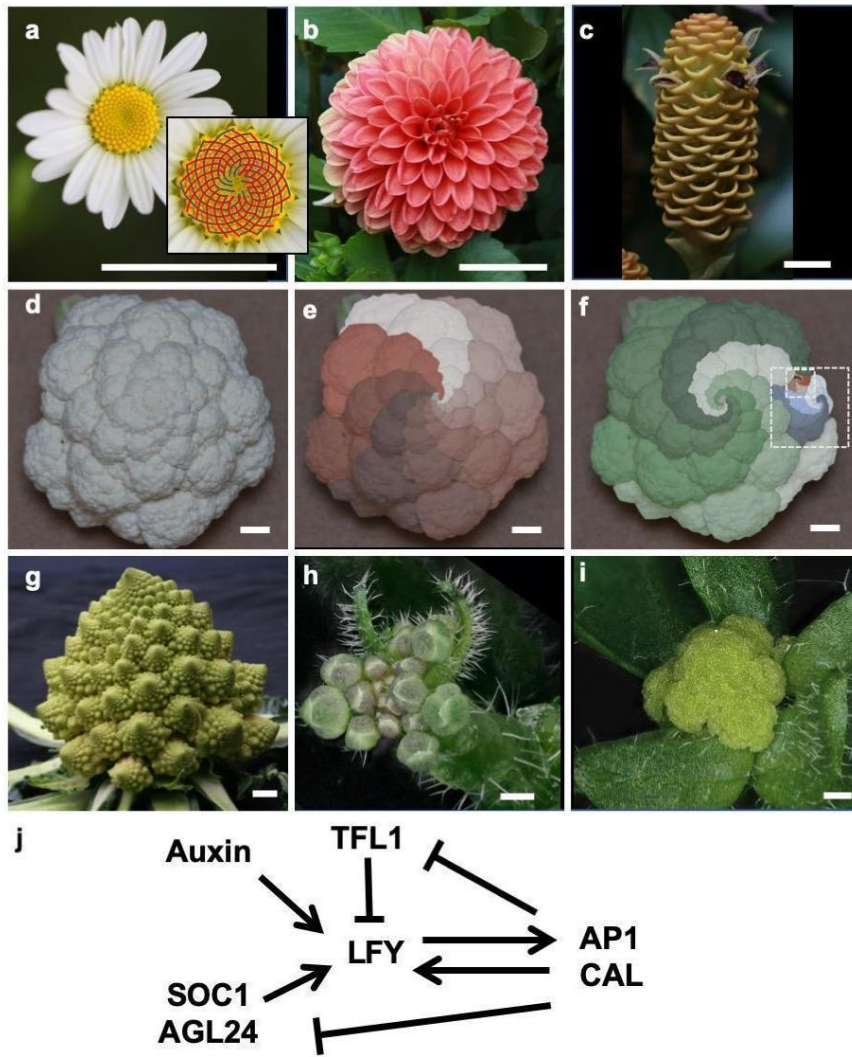
49 Above-ground plant architectures arise from activity of shoot apical meristems (SAM), which
50 are pools of stem cells that give rise to organs such as leaves, shoots or flowers. The arrangement
51 of organs on stems is termed phyllotaxis. Plants with a spiral phyllotaxis usually form two
52 families of organ spirals, visible on compact structures such as flower heads, pine cones or cacti
53 (Fig. 1a-c). These two families of spirals turn in opposite directions, and come in two
54 consecutive numbers of the Fibonacci series (Fig. 1a) (1). In cauliflowers, spiral families are
55 visible not only at one but at several scales (Fig. 1d-f). This self-similar organization culminates
56 in the Romanesco cultivar where the spirals appear in relief due to their conical shape at all
57 scales, a geometrical feature conferring the whole curd a marked fractal-like aspect (Fig. 1g).

58

59 Cauliflowers (*Brassica oleracea* var. *botrytis*) were domesticated from cabbages (2). The
60 cauliflower inflorescence (the shoot bearing flowers) takes a curd shape because each emerging

61 flower primordia never matures to the floral stage but instead generates more curd-shaped
62 inflorescences (2, 3). In *B. oleracea*, the genetic modifications causing curd development are still
63 debated and likely affect multiple genes (2–5). However, cauliflower-like structures also exist in
64 the model brassicaceae *Arabidopsis thaliana* and are caused by a double mutation in *APETALA1*
65 (*API*) and *CAULIFLOWER* (*CAL*) (Fig. 1h-i), two paralogous genes encoding MADS-box
66 transcription factors (TF) promoting floral development (6, 7). The *Arabidopsis* molecular
67 regulators governing the development of shoots and flowers have been largely identified (8–
68 10)(Table S1). Network models based on these regulators have been proposed to explain wild-
69 type flower development (11–14). However, whether variants of these networks are able to
70 account for development of *Arabidopsis apl cal* curds is unknown.

71
72 To address this question, we first built a network of the main regulators involved in both flower
73 and curd development. Then, we embedded this network within a 3D computational model of
74 plant development to understand how mutations could transform wild-type (WT) inflorescences
75 into curds.



76

77 **Figure 1: Illustrations of phyllotactic spirals on plant inflorescences**

78 (a) Daisy capitulum: the two families of spirals are indicated in the close-up (13 blue spirals and
 79 21 red). (b) Dahlia composite flower (c) Zingiber inflorescence. (d-f) *Brassica oleracea* var.
 80 *botrytis* cauliflower with (e) 8 counterclockwise (brown family) and (f) 5 clockwise (green
 81 family) main spirals. Dashed rectangles show families of spirals nested over several scales (g)
 82 Romanesco curd, (h) Arabidopsis wild-type inflorescence (h) and *ap1 cal* curd (i), Bar = 2 cm (a-
 83 g), 500 μ m (h-i). (j) Interactions between major floral regulators; arrows depict activation
 84 whereas barred lines indicate repression.

85

86

87

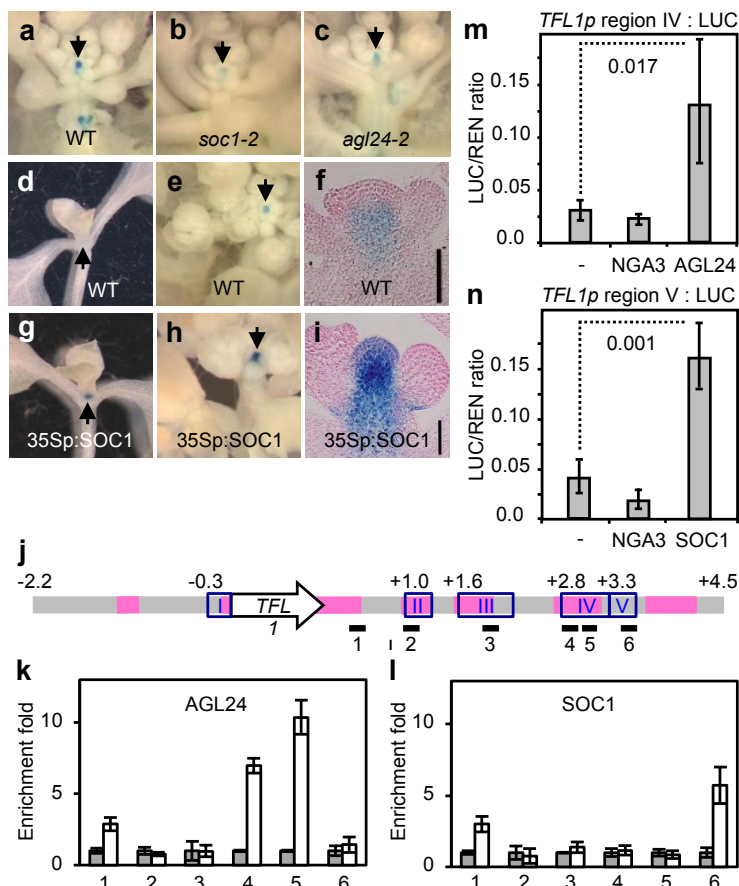
88 **The genetic basis of cauliflower curds**

89 In Arabidopsis, flowers are initiated by the TF LEAFY (LFY) (Fig. 1j) (Table S1). *LFY* is
90 upregulated by the SUPPRESSOR-OF-OVEREXPRESSION-OF-CO 1 (SOC1) and
91 AGAMOUS-LIKE 24 (AGL24) MADS-box proteins (induced throughout the inflorescence
92 meristem by environmental and endogenous cues) and by auxin phytohormone maxima that
93 mark floral meristem initiation sites. *LFY* is expressed specifically in floral primordia because its
94 induction in the SAM is repressed by the TFL1 inflorescence identity protein. In the floral
95 primordium, LFY induces *API* and *CAL* (*API/CAL*) that positively feedback on *LFY* and repress
96 both *SOC1/AGL24* and *TFL1*, thereby stabilizing the floral fate of the new meristem. In the *apl*
97 *cal* cauliflower mutant, the API/LFY positive feedback is absent and *TFL1* is not repressed by
98 API/CAL in the nascent floral meristem. Consequently, young flower primordia cannot maintain
99 *LFY* expression and start themselves expressing *TFL1*. As a result, they lose their floral identity
100 and become inflorescence meristems (6). Whereas *TFL1* repression in nascent flower primordia
101 is well understood, the factors directly responsible for its upregulation in *apl cal* and
102 inflorescence meristems are unknown.

103
104 To complete our network, we thus searched for direct positive regulators of *TFL1*, other than
105 LFY (that induces *TFL1* (15) but is not active in inflorescence meristems). *TFL1* is indirectly
106 regulated by day length (16): in long days (LD) *TFL1* is up-regulated by CONSTANS (CO) and
107 FT, two key upstream effectors of the LD pathway (11, 17–19) (Fig. S1). To search for direct
108 regulators, we examined SOC1 and AGL24 that act downstream of CO and FT in the LD
109 pathway (9). Loss- and gain-of-function experiments demonstrated that both SOC1 and AGL24
110 induce *TFL1* (Fig. 2a-i) and Chromatin Immuno-Precipitation showed that these two TFs bind to
111 the *TFL1* regions that regulate its expression in the SAM (20) (Fig. 2j-l). These regions were
112 sufficient to activate a *TFL1* reporter construct by SOC1 and AGL24 in a transient assay (Fig.
113 2m-n) confirming that both MADS-box TFs are direct regulators of *TFL1*. Since XAANTAL2
114 (XAL2), a homolog of SOC1 and AGL24 also bound to and induced *TFL1* (21), we aggregated
115 the activities of SOC1, AGL24 and XAL2 into a SAX proxy acting as *TFL1* positive regulator
116 (Fig. 3a).

117

118 We thus created the SALT network (for SAX, AP1/CAL, LFY, and TFL1; Fig. 3a) made of
 119 these 4 regulator sets, auxin (22), and F, a flower inducing signal (a proxy for the FT florigen)
 120 that increases when the plant ages or is exposed to flower-inducing environmental conditions
 121 (23, 24). We also added a short-lived transient early Repressor of *TFL1* (eREP), as a proxy for
 122 *TFL1* early repression in the young flower bud performed by the redundant activities of SOC1,
 123 AGL24, SHORT VEGETATIVE PHASE, and SEPALLATA4 (25).



124
 125 **Fig. 2: AGL24 and SOC1 are direct positive regulators of *TFL1*.**
 126 (a-c), *TFL1p*:GUS activity in WT (a), *soc1-2* (b) and *agl24-2* (c) inflorescence apices. (d-i),
 127 *TFL1p*:GUS activity (blue signal) in WT (d-f) and *35Sp:SOC1* (g-i) apices at vegetative (d,g)
 128 and flowering (e,f,h,i) stages. (f-i), longitudinal sections through flowering shoots. Arrows mark
 129 the SAM. Scale bars in (f) and (i), 40 μ m. (j-l) Structure of *TFL1* locus, with regions conserved
 130 in Brassicaceae (pink lines), regulatory regions (20) (blue boxes I-V), and fragments used in
 131 ChIP (black lines 1-6). ChIP experiments on plants expressing a tagged version of AGL24 (k,

132 white bars) or the WT SOC1 protein (l, white bars) or on control plants (grey bars, see Material
133 and Methods), show that AGL24 binds region IV (k, fragments 4-5) and SOC1 region V (l,
134 fragment 6). A representative biological replicate is shown with the mean \pm SE for three
135 technical replicates. (m,n) Transient assays showing transactivation of the LUCIFERASE (LUC)
136 reporter driven by region IV (activation by 35Sp:AGL24) and region V (activation by
137 35Sp:SOC1). NGA3 is an unrelated TF used as negative control. Bars denote the mean and
138 standard deviation of three independent biological replicates. *P* values are for the equality of
139 means (Student's t-test).

140

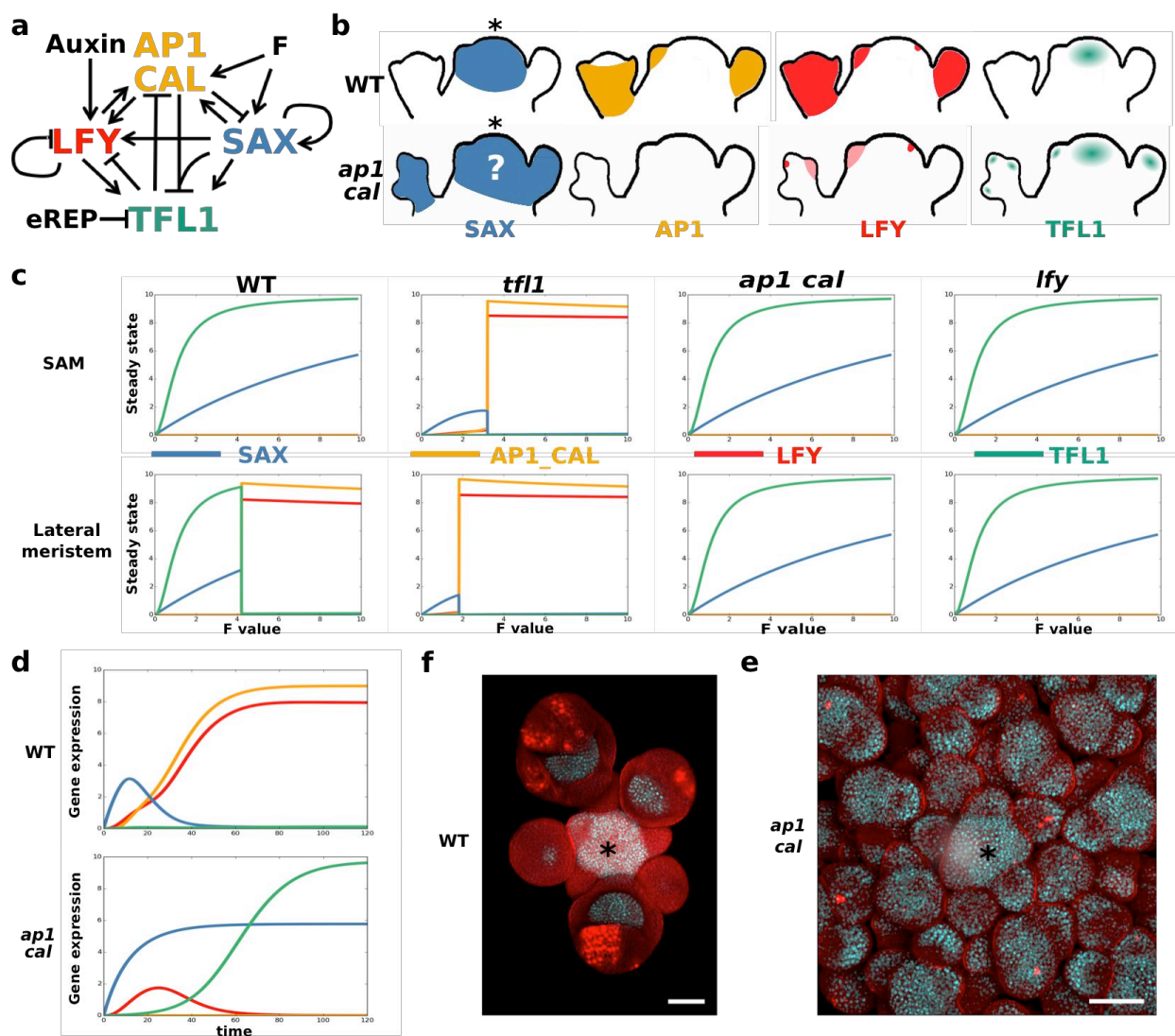
141 The steady states of the SALT network correspond to the gene expression patterns observed in
142 wild-type vegetative (low SALT values), inflorescence (high TFL1/SAX, low AP1/CAL/LFY)
143 and flower (low TFL1/SAX, high AP1/CAL/LFY) meristems (Fig. 3b,c, Fig. S2). Above an *F*
144 threshold value, the network generates a flower or an inflorescence state depending on *F* and
145 auxin values. Simulations of *tfl1*, *lfy*, *ap1 cal* mutants produce expected outputs consistent with
146 experimentally reported gene expressions (6, 16, 26, 27) (Fig. 3b, c). The simulated *sax* mutant
147 did not reach a floral state, consistent with the late flowering behavior of the *soc1 agl24* double
148 mutant (28).

149

150 The modelled gene expression dynamics (Fig. 3d) illuminate the fundamental differences
151 between WT and cauliflower meristems: in a WT flower primordium, *F* induces *SAX*. *SAX* and
152 auxin induce *LFY*, that, together with *F*, induce *API/CAL*. *API* positively feeds back on *LFY* and
153 represses *SAX* (Fig. 3d). *TFL1* expression, that could be induced by *SAX* and *LFY* in early floral
154 stages, is constantly repressed, first by eREP and later by *SAX* plus *API/CAL*. High *API/CAL*
155 and *LFY* with low *TFL1* and *SAX* expression stabilize the floral fate. In contrast, in the *ap1 cal*
156 flower primordia, the absence of *API/CAL* activity has two consequences: i) *LFY* expression is
157 upregulated only transiently since *API/CAL* positive feedback is missing (Fig. 3d) and ii) *SAX*
158 genes are not repressed by *API* and thus induce *TFL1* in nascent flower meristems. *TFL1*
159 represses *LFY* even further and the meristem returns to a shoot meristem state (Fig. 3d). Note
160 that, the early *LFY* induction would likely be reinforced (while remaining transient) by
161 incorporating the recently discovered direct induction of *LFY* by the *F* partner protein *FD* (29).
162 The SALT model predicts that *SAX* expression should extend over the entire cauliflower. We

163 analyzed a SOC1-GFP reporter line and indeed observed expansion of its expression domain in
 164 *ap1 cal* as compared to WT (Fig. 3e, f).

165



166

167 **Fig. 3: SALT Gene Regulatory Network model and experimental validation.**

168 (a) SALT GRN network structure (b) Known expression patterns of *SAX*, *AP1/CAL*, *LFY*, and
 169 *TFL1* in the SAM and lateral primordia of WT and *ap1 cal* mutant. The question mark indicates
 170 a predicted expression pattern of the model. (c) WT, *tfl1*, *ap1 cal* and *lfy* steady states of the
 171 model at different F values in the SAM (low auxin) and in lateral meristems (high auxin). The
 172 genetic identity predicted for WT and all mutant meristems correspond to the experimentally
 173 observed phenotypes. (d) Temporal simulation of gene expression in lateral primordia with high

174 F value. (e, f) Expression of the SOC1:GFP (white/light blue signal) reporter construct in WT (e)
175 and in the *ap1-7 cal-1* mutant (f) inflorescences. Asterisks mark the SAM. Bar = 50 μ m.

176
177 The SALT network thus recapitulates realistic gene expressions driving meristem fates.
178 However, a plant architecture does not only depend on meristem fates but also on
179 morphodynamic parameters including molecular thresholds for fate decisions, organ growth rate,
180 delay for meristems to start organ production and organ production rate which are independently
181 regulated. Plant inflorescence architecture thus emerges from the complex interaction between
182 the floral GRN and morphodynamic parameters. This is illustrated here by the *lfy* and *ap1 cal*
183 mutants that have the same GRN outputs (Fig. 3c) but markedly different architectures (6, 27).
184 To study how this interaction operates in Arabidopsis, we integrated the SALT GRN in a 3D
185 plant computational model implemented as an L-system (see Supplementary materials Modeling
186 Methods).

187
188 **A multi-scale model generates Arabidopsis cauliflower structures**

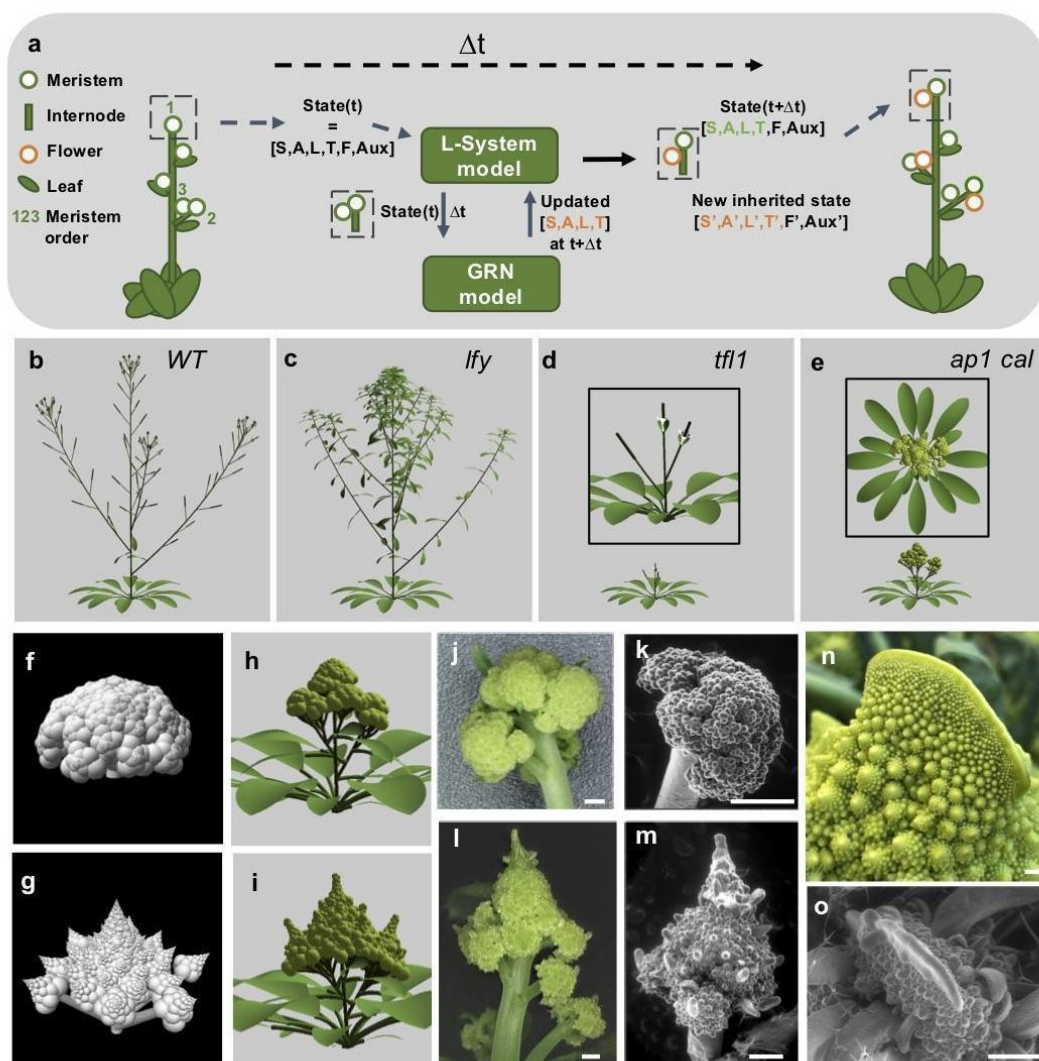
189 The 3D model is made of the 4 types of organs that shape plant above-ground architecture:
190 meristems, internodes, leaves and flowers (Fig. 4a, Supplementary materials). Each meristem's
191 identity (vegetative, inflorescence and floral) is determined by the GRN steady state, computed
192 at each time step as a function of the meristem's previous state and external factors (auxin and
193 F). The GRN model is implemented as single compartment ordinary differential equations
194 (Supplementary materials Modeling Methods). We assume that the GRN dynamics is faster than
195 growth and reaches its steady state within a time step. A set of growth rules defines meristem
196 production: a vegetative meristem produces a compressed stem (non-elongated internodes) with
197 rosette leaves; an inflorescence meristem produces an elongating internode, a cauline leaf and a
198 new shoot meristem in the leaf axil; a floral meristem produces an internode terminating with a
199 flower meristem, devoid of bracts (leaf-like organs subtending flowers) since they are repressed
200 by LFY (6)). Each newly generated axillary meristem begins with maximal auxin level (22),
201 SAX/LFY/AP1/CAL values inherited from the parent meristem, together with a fraction of the
202 parent TFL1 value as, in the real plant, this non-cell autonomous protein is present in the
203 primordia region (30). To match the wild-type plant architecture, indeterminate meristems at
204 orders >2 (Fig. 4a) were kept quiescent, a likely effect of apical dominance (the inhibition of

205 lateral meristem outgrowth) (Fig. S3a). The model also contains rules describing organ growth
206 dynamics (internode and leaf elongation, flower growth, organ production rate, growth initiation
207 delay). Simulated plants start with a single vegetative SAM and repeatedly produce new organs
208 according to the GRN, the morphodynamic rules and an input value of F.

209 By adjusting the GRN and morphodynamic parameters within a range of plausible values
210 (Supplementary materials), we successfully calibrated the model to produce realistic
211 architectures for wild-type and *lfy* plants (Supplementary Movies 1-2), as well as for the *tfl1*
212 mutant (Fig. 4b-d) and a non-flowering phenotype for the *sax* mutant. However, our simulations
213 could not generate a realistic *apl cal* mutant growing without bract/cauline leaves and displaying
214 high order meristems (Fig. S3a-b) suggesting that the cauliflower phenotype involves additional
215 regulations. We reasoned that laterally produced *apl cal* inflorescence meristems are different
216 from those produced in other genotypes as, according to our GRN, they have been transiently
217 exposed to LFY expression (Fig. 3d). Several pieces of evidence suggest that this transient LFY
218 expression, already known to repress bracts (6), could also contribute to high-order meristem
219 release. First, the outgrowth of otherwise inhibited axillary meristems in the rosette is stimulated
220 by ectopic expression of LFY (or a LFY allele) (31, 32). Second, it was established that the *lfy*
221 *apl cal* triple mutant does not form cauliflowers (6) and we found that, in this mutant, the
222 number of high-order meristems is significantly reduced as compared to *apl cal* (Fig. S3d-h),
223 thus supporting our hypothesis.

224 We abstracted this critical molecular pathway, by introducing in the model a factor X
225 upregulated when LFY exceeds a minimal threshold level. Upregulated factor X releases high-
226 order meristem growth and suppresses the bract. This was sufficient to unlock the recursive
227 growth of lateral meristems and to generate the *apl cal* curd structure that arises from the
228 transient but irreversible exposure of meristems to the floral signal without any alteration of wild
229 type growth dynamics (Fig. 4e,h, Supplementary Movie 3). Overall, our work shows that the *apl*
230 *cal* and *lfy* architectures are different (Fig. 3c) because the molecular histories of their
231 inflorescence meristems are different, thereby revealing the existence of a developmental
232 hysteresis.

233



234

235 **Fig. 4: Simulation and assessment of a GRN-based plant development model.**

236 (a) Schematic representation of the multi-scale model of Arabidopsis development. Each
 237 meristem state is composed of signal levels (auxin, F) and a GRN steady state. At time t , the
 238 plant is made up of a collection of organs (left). At time $t+\Delta t$ (right) the model updates the signal
 239 levels and GRN state in each meristem. The steady state defines the identity of the meristems
 240 (vegetative, inflorescence or flower) used to compute meristem lateral productions. Green
 241 numbers indicate meristem order (b-e). Plant morphologies obtained in the WT (b), *lfy* (c), *tfl1*
 242 (d) and *ap1 cal* (e) simulations. Simulated morphologies with constant (f,h) or increased
 243 meristem size (g,i) in a simplified (f,g) and the Arabidopsis model (h,i). Light micrographs (j,l,n)
 244 and s.e.m (k,m,o) of cauliflower structures in Arabidopsis *ap1 cal* (j, k), Arabidopsis *ap1 cal*

245 *chl3* (l, m, o) and Romanesco (n). Uninduced *API:GR* transgene is present in plants j-m. Scale
246 bars = 500 μm .

247

248 **Growth dynamics define cauliflower and Romanesco curd structures**

249 Our work in *Arabidopsis* offers a conceptual framework to explain how inflorescence
250 architecture emerges from coupling a floral GRN to morphodynamic parameters. We wondered
251 whether modifications affecting components of this framework could also explain the
252 architecture of the cauliflowers that arose during domestication, namely the edible *Brassica*
253 *oleracea* (*Bo*) var. *botrytis* (*Bob*) and its Romanesco variant. Whether similar genetic defects as
254 in *Arabidopsis* are responsible for curd development in *B. oleracea* is still debated (4, 5). To
255 further investigate this point, we analysed RNA-seq data of *Bob* curds: we confirmed the
256 previously identified mutation in the *BobCAL* gene (Fig. S4a)(4, 5, 7) and observed that the two
257 *API* paralogs (*BobAPI-a* and *BobAPI-c*) are expressed at much lower levels than in cabbage (*Bo*
258 var. *capitata*) inflorescences (Fig. S4b). These functional proteins are induced with a delay only
259 when the cauliflower elongates and start forming normal flowers (3, 33). Comparing cauliflower
260 and cabbage sequences, we identified differences in binding sites for candidate regulators of
261 *BoAPI* that could account for their delayed activation (Fig. S4d). The combination of *BoCAL*
262 inactivation and *BobAPI-a/c* expression delay (heterochrony due to *cis* or *trans* mutations) thus
263 likely participates to *Bob* curd development. Similar to *Arabidopsis ap1 cal*, cauliflowers have
264 meristems of higher maximal order ($n \geq 7$) than cabbages ($n = 3-4$) (Fig. S5). Nevertheless, the
265 development of single massive cauliflower curds is not the exact equivalent of the *Arabidopsis*
266 mutant (3, 5) and involves additional multifactorial alterations of morphodynamics parameters
267 (such as reduction of internode elongation and branches diameter increase).

268

269 The conical shapes appearing in Romanesco spirals at all scales (Fig. 1f) represent an additional
270 geometric variation obtained through domestication that seems to be associated with a change in
271 morphodynamic parameters. Indeed, several such parameters remain constant during cauliflower
272 development but vary in Romanesco (34): i) the plastochron, the time between two successive
273 meristem productions, ii) the number of visual spirals originating from a given meristem, iii) the
274 time (measured in number of plastochrons) needed before a lateral primordium starts producing
275 its own primordia (or lateral production onset delay), and iv) the size of the meristems. Whether

276 some of these parameters are causal to the Romanesco phenotype remains unclear but
277 phyllotaxis studies (1, 35, 36) indicate that the first three parameters are linked to the meristem
278 size: an augmentation of the size of the meristem central zone should decrease the plastochron,
279 which in turn increases the number of spirals, and the lateral production onset delay. We thus
280 hypothesized that passing from a constant to a decreasing plastochron in meristems could change
281 cauliflower into Romanesco morphologies. We first tested this *in silico* using a simplified, purely
282 geometric model of curd growth, independent from the Arabidopsis GRN and specific growth
283 dynamics (Supplementary materials). A decreasing plastochron was sufficient to produce
284 Romanesco shapes (Fig. 4g) whereas constant values of this parameter produce cauliflower
285 morphologies (Fig. 4f).

286
287 We then introduced the same change in the more complex GRN-based, Arabidopsis cauliflower
288 architectural model, while keeping its organ growth dynamics as calibrated on the WT. Although
289 not as complete as in the purely geometric model, the curd changed towards a “Romanesco-like”
290 morphology with typical conical curd shapes (Fig. 4h, i). We then tested this hypothesis
291 experimentally in Arabidopsis by altering the size of the meristem directly. We achieved this by
292 introducing a mutation in the *CLAVATA3 (CLV3)* gene that controls meristem homeostasis and
293 induces an increase of the meristem central zone during growth (37, 38). As predicted by our
294 analysis, introduction of a *clv3* mutation in *ap1 cal* Arabidopsis mutant modified the curd shape,
295 which lost its round morphology and acquired a more conical shape, with similar structures at
296 different scales, features recognized as hallmarks of Romanesco curds (39) (Fig. 4l-m). Two
297 additional pieces of evidence support the hypothesis that meristem homeostasis is perturbed in
298 Romanesco curds: they occasionally show fasciation, a feature typical of meristem enlargement
299 also observed in *clv3* or *ap1 cal clv3* mutants (Fig. 4n,o)(37). Moreover, the expression of *CLV3*
300 (and possibly two other genes acting in the same pathway)(38) are lower in Romanesco curds
301 than in cauliflowers (Fig. S6). Altogether, these observations establish that meristem size
302 regulates the final curd morphology through control of plastochron value.

303
304 These results reveal how fractal patterns can be generated through growth and developmental
305 networks that alter identities and meristem dynamics. Our data, GRN and growth models now
306 clarify the molecular and morphological changes over time by which meristems gain different

307 identities to form the highly diverse and fascinating array of plant architectures found throughout
308 nature and crops.

309

310 **References and Notes:**

311

- 312 1. C. Godin, C. Golé, S. Douady, *Development*. **147**, dev165878 (2020).
- 313 2. C. F. Quiros, M. W. Farnham, in *Genetics and Genomics of the Brassicaceae*, R. Schmidt,
314 I. Bancroft, Eds. (Springer New York, 2011), pp. 261–289.
- 315 3. D. V. Duclos, T. Björkman, *J. Exp. Bot.* **59**, 421–433 (2008).
- 316 4. L. B. Smith, G. J. King, *Mol. Breeding*. **6**, 603–613 (2000).
- 317 5. N. Guo, S. Wang, L. Gao, Y. Liu, X. Wang, E. Lai, M. Duan, G. Wang, J. Li, M. Yang,
318 M. Zong, *BMC Biology*. **19**, 93 (2021).
- 319 6. J. L. Bowman, J. Alvarez, D. Weigel, E. M. Meyerowitz, D. R. Smyth, *Development*. **119**,
320 721 (1993).
- 321 7. S. Kempin, B. Savidge, M. Yanofsky, *Science*. **267**, 522 (1995).
- 322 8. G. Denay, H. Chahtane, G. Tichtinsky, F. Parcy, *Curr. Opin. Plant Biol.* **35**, 15–22 (2017).
- 323 9. A. Pajoro , S. Biewers, E. Dougali, F. Leal Valentim, M. A. Mendes ,A. Porri, G.
324 Coupland, Y. Van de Peer, A.D. Van Dijk, L. Colombo, B. Davies, *J. Exp. Bot.* **65**, 4731–
325 4745 (2014).
- 326 10. B. Thomson, F. Wellmer, *Curr. Top. Dev. Biol.* **131**, 185–210 (2019).
- 327 11. K. E. Jaeger, N. Pullen, S. Lamzin, R. J. Morris, P. A. Wigge, *Plant Cell*. **25**, 820 (2013).
- 328 12. C. Espinosa-Soto, P. Padilla-Longoria, E. R. Alvarez-Buylla, *Plant Cell*. **16**, 2923–2939
329 (2004).
- 330 13. F. L. Valentim *et al.*, *PLOS ONE*. **10**, e0116973 (2015).
- 331 14. P. Prusinkiewicz, Y. Erasmus, B. Lane, L. D. Harder, E. Coen, *Science*. **316**, 1452 (2007).
- 332 15. K. Goslin *et al.*, *Plant Physiol.* **174**, 1097 (2017).
- 333 16. C. Ferrandiz, Q. Gu, R. Martienssen, M. F. Yanofsky, *Development*. **127**, 725 (2000).
- 334 17. D. Bradley, O. Ratcliffe, C. Vincent, R. Carpenter, E. Coen, *Science*. **275**, 80 (1997).
- 335 18. X. Hou *et al.*, *Nat. Commun.* **5**, 4601 (2014).
- 336 19. S. K. Yoo *et al.*, *Plant Physiol.* **139**, 770 (2005).

- 337 20. A. Serrano-Mislata *et al.*, *Development*. **143**, 3315 (2016).
- 338 21. R. V. Pérez-Ruiz *et al.*, *Mol. Plant*. **8**, 796–813 (2015).
- 339 22. D. Reinhardt *et al.*, *Nature*. **426**, 255–260.
- 340 23. P. A. Wigge, *Curr. Biol*. **21**, R374-378 (2011).
- 341 24. J. Putterill, E. Varkonyi-Gasic, *Curr. Opin. Plant Biol*. **33**, 77–82 (2016).
- 342 25. C. Liu *et al.*, *Dev. Cell*. **24**, 612–622 (2013).
- 343 26. O. J. Ratcliffe *et al.*, *Development*. **125**, 1609 (1998).
- 344 27. D. Weigel, J. Alvarez, D. R. Smyth, M. F. Yanofsky, E. M. Meyerowitz, *Cell*. **69**, 843–
345 859 (1992).
- 346 28. S. D. Michaels *et al.*, *Plant J*. **33**, 867–874 (2003).
- 347 29. Y. Zhu *et al.*, *Nat. Commun*. **11**, 5118 (2020).
- 348 30. L. Conti, D. Bradley, *Plant Cell*. **19**, 767 (2007).
- 349 31. H. Chahtane *et al.*, *Plant J*. **74**, 678–689 (2013).
- 350 32. D. Weigel, O. Nilsson, *Nature*. **377**, 495–500 (1995).
- 351 33. X. Sun *et al.*, *Environ. Exp. Bot.* **155**, 742–750 (2018).
- 352 34. M. Kieffer, M. P. Fuller, A. J. Jellings, *Planta*. **206**, 34–43 (1998).
- 353 35. S. Douady, Y. Couder, *J. Theor. Biol*. **178**, 255–273 (1996).
- 354 36. Y. Refahi *et al.*, *eLife*. **5**, e14093 (2016).
- 355 37. J. C. Fletcher, *Science*. **283**, 1911–1914 (1999).
- 356 38. M. Kitagawa, D. Jackson, *Annu. Rev. Plant Biol*. **70**, 269–291 (2019).
- 357 39. L. E. Watts, *Euphytica*. **15**, 111–115 (1966).
- 358 40. A. Maizel, D. Weigel, *Plant J*. **38**, 164–171 (2004).
- 359 41. V. Grandi, V. Gregis, M. M. Kater, *Plant J*. **69**, 881–893 (2012).
- 360 42. R. G. H. Immink *et al.*, *Plant Physiol*. **160**, 433 (2012).
- 361 43. I. Kardailsky, *Science*. **286**, 1962–1965 (1999).
- 362 44. H. Lee, *Genes Dev*. **14**, 2366–2376 (2000).

- 363 45. V. Gregis, A. Sessa, C. Dorca-Fornell, M. M. Kater, *Plant J.* **60**, 626–637 (2009).
- 364 46. H. Onouchi, M. I. Igeño, C. Périlleux, K. Graves, G. Coupland, *Plant Cell.* **12**, 885–900
365 (2000).
- 366 47. M. Koornneef, C. J. Hanhart, J. H. van der Veen, *Mol. Gen. Genet.* **229**, 57–66 (1991).
- 367 48. F. Wellmer, M. Alves-Ferreira, A. Dubois, J. L. Riechmann, E. M. Meyerowitz, *PLoS*
368 *Genet.* **2**, e117 (2006).
- 369 49. R. A. Jefferson, T. A. Kavanagh, M. W. Bevan, *EMBO J.* **6**, 3901–3907 (1987).
- 370 50. N. Bechtold, J. Ellis, G. Pelletier, *C. R. Acad. Sci. Paris, Life Sci.* **316**, 1194–1199 (1993).
- 371 51. N. Bechtold, D. Bouchez, in *Gene Transfer to Plants*, I. Potrykus, G. Spangenberg, Eds.
372 (Springer Berlin Heidelberg, 1995) pp. 19–23.
- 373 52. M. Trigueros *et al.*, *Plant Cell.* **21**, 1394–1409 (2009).
- 374 53. I. Mitsuhashi *et al.*, *Plant Cell Physiol.* **37**, 49–59 (1996).
- 375 54. R. Hellens *et al.*, *Plant Methods.* **1**, 13 (2005).
- 376 55. Z. Feng *et al.*, *Cell Res.* **23**, 1229–1232 (2013).
- 377 56. W. Yan, D. Chen, K. Kaufmann, *Plant Methods.* **12**, 23 (2016).
- 378 57. S. Bensmihen *et al.*, *FEBS Lett.* **561**, 127–131 (2004).
- 379 58. S. J. Clough, A. F. Bent, *Plant J.* **16**, 735–743 (1998).
- 380 59. N. Prunet, K. Duncan, *J. Exp. Bot.* **71**, 2898–2909 (2020).
- 381 60. A. Sessions, D. Weigel, M. F. Yanofsky, *Plant J.* **20**, 259–263 (1999).
- 382 61. D. Weigel, J. Glazebrook, *Arabidopsis: a laboratory manual* (Cold Spring Harbor
383 Laboratory Press, New York, 2002).
- 384 62. C. Dorca-Fornell *et al.*, *Plant J.* **67**, 1006–1017 (2011).
- 385 63. C. Belser *et al.*, *Nat. Plants.* **4**, 879–887 (2018).
- 386 64. J. Yu *et al.*, *BMC Genomics.* **15**, 3 (2014).
- 387 65. H. Lv *et al.*, *Sci Rep.* **10**, 12394 (2020).
- 388 66. O. Fornes *et al.*, *Nucleic Acids Res.* **48**, D87–D92 (2019).
- 389 67. E. Moyroud *et al.*, *Plant Cell.* **23**, 1293 (2011).

- 390 68. B. H. Toyama, M. W. Hetzer, *Nat. Rev. Mol. Cell Bio.* **14**, 55–61 (2013).
- 391 69. A. Jolma *et al.*, *Nature*. **527**, 384–388 (2015).
- 392 70. S. Legewie, H. Herzel, H. V. Westerhoff, N. Blüthgen, *Mol. Syst. Biol.* **4**, 190 (2008).
- 393 71. S. Belikov, O. G. Berg, Ö. Wrangé, *Nucleic Acids Res.* **44**, 3045–3058 (2015).
- 394 72. S. Mangan, U. Alon, *Proc. Natl. Acad. Sci. U.S.A.* **100**, 11980–11985 (2003).
- 395 73. P. Prusinkiewicz, A. Lindenmayer, *The algorithmic beauty of plants* (Springer-Verlag,
396 New York, 1990).
- 397 74. F. Boudon, C. Pradal, T. Cokelaer, P. Prusinkiewicz, C. Godin, *Front. Plant Sci.* **3** (2012).
- 398 75. L. Mündermann, Y. Erasmus, B. Lane, E. Coen, P. Prusinkiewicz, *Plant Physiol.* **139**,
399 960–968 (2005).
- 400 76. C. M. Winter *et al.*, *Dev. Cell.* **20**, 430–443 (2011).
- 401 77. D. A. Williams *et al.*, *Proc. Natl. Acad. Sci. U.S.A.* **101**, 1775 (2004).
- 402 78. R. Benlloch *et al.*, *Plant J.* **67**, 1094–1102 (2011).
- 403 79. D. Wagner, R. W. M. Sablowski, E. M. Meyerowitz, *Science*. **285**, 582 (1999).
- 404 80. F. Parcy, O. Nilsson, M. A. Busch, I. Lee, D. Weigel, *Nature*. **395**, 561 (1998).
- 405 81. S. Hanano, K. Goto, *Plant Cell.* **23**, 3172 (2011).
- 406 82. O. J. Ratcliffe, D. J. Bradley, E. S. Coen, *Development*. **126**, 1109 (1999).
- 407 83. D. Goretti *et al.*, *Plant Physiol.*, **182** 2081-2095 (2020).
- 408 84. J.-H. Jung, H.-J. Lee, J. Y. Ryu, C.-M. Park, *Mol. Plant.* **9**, 1647–1659 (2016).
- 409 85. P. A. Wigge *et al.*, *Science*. **309**, 1056 (2005).
- 410 86. S. Collani, M. Neumann, L. Yant, M. Schmid, *Plant Physiol.* **180**, 367–380 (2019).
- 411 87. M. Abe, *Science*. **309**, 1052–1056 (2005).
- 412 88. P. Teper-Bamnolker, A. Samach, *Plant Cell.* **17**, 2661–2675 (2005).
- 413 89. M. Romera-Branchat *et al.*, *Cell Rep.* **31**, 107717 (2020).
- 414 90. S.J. Liljegren, C. Gustafson-Brown, A. Pinyopich, G. S. Ditta, M. F. Yanofsky, *Plant Cell.*
415 **11**, 1007 (1999).

- 416 91. K. Kaufmann *et al.*, *Science*. **328**, 85 (2010).
- 417 92. J. Lee, M. Oh, H. Park, I. Lee, *Plant J.* **55**, 832–843 (2008).
- 418 93. J. Moon, H. Lee, M. Kim, I. Lee, *Plant Cell Physiol.* **46**, 292–299 (2005).
- 419 94. C. Liu *et al.*, *Development*. **135**, 1481 (2008).
- 420 95. N. Yamaguchi *et al.*, *Dev Cell*. **24**, 271–282 (2013).
- 421 96. W. Li *et al.*, *Sci. Signal.* **6**, ra23 (2013).
- 422 97. O. Nilsson, I. Lee, M. A. Blázquez, D. Weigel, *Genetics*. **150**, 403–410 (1998).
- 423 98. A. Serrano-Mislata *et al.*, *Plant Signal. Behav.* **12**, e1370164 (2017).
- 424 99. C. Liu *et al.*, *Development*. **134**, 1901 (2007).
- 425 100. H. Yu, T. Ito, F. Wellmer, E. M. Meyerowitz, *Nat. Genet.* **36**, 157 (2004).
- 426 101. Z. Tao *et al.*, *Plant J.* **70**, 549–561 (2012).
- 427 102. H. Yu, Y. Xu, E. L. Tan, P. P. Kumar, *Proc. Natl. Acad. Sci. U.S.A.* **99**, 16336–16341
428 (2002).
- 429 103. J.-W. Wang, B. Czech, D. Weigel, *Cell*. **138**, 738–749 (2009).
- 430 104. S. D. Michaels, E. Himelblau, S. Y. Kim, F. M. Schomburg, R. M. Amasino, *Plant*
431 *Physiol.* **137**, 149–156 (2005).
- 432 105. I. Searle, *Gene. Dev.* **20**, 898–912 (2006).
- 433 106. R. Borner *et al.*, *Plant J.* **24**, 591–599 (2000).
- 434 107. A. Samach, *Science*. **288**, 1613–1616 (2000).
- 435 108. S. R. Hepworth, *The EMBO J.* **21**, 4327–4337 (2002).

436

437 **Acknowledgments**

438 We thank Anne-Marie Chèvre, Richard Immink, Rüdiger Simon, Lars Ostergaard and Mariana
439 Benitez for advice, Teva Vernoux, Chloe Zubieta and Hicham Chahtane for proofreading and
440 useful feedback on the manuscript, Dominique Tardy, Eric Giraud, Renaud Dumas and Vincent
441 Martin (OBS, France) for providing cauliflower samples and Lydia Bousset Vaslin for images
442 and branch counting, Frédéric Boudon for help with L-Py, Richard Immink (Wageningen,
443 Netherlands), C. Ferrándiz (IBMCP; Spain), George Coupland (MPIPZ, Germany), Miguel

444 Ángel Blázquez (IBMCP, Spain), Richard Amasino (UWM, USA) and the European
 445 Arabidopsis Stock Centre for providing seeds, Vincent Berger (CEA/DRF) for the Keyence
 446 microscope, Christine Lancelon-Pin (Plateau de microscopie électronique - ICMG. CERMAV-
 447 CNRS) for SEM experiments.

448

449 **Funding**

450 This project received support from the INRAE Caulimodel project (FP and CG), Inria Project
 451 Lab Morphogenetics (CG, EA and FP), the ANR BBSRC Flower model project (FP and CG), the
 452 GRAL LabEX (ANR-10-LABX-49-01) with the frame of the CBH-EUR-GS (ANR-17-EURE-
 453 0003), EU H2020 773875 ROMI project funding (CG), the Spanish Ministerio de Ciencia
 454 Innovación and FEDER (grant no. PGC2018-099232-B-I00)(FM).

455

456 **Author contributions**

457 ChG and FP conceived the study

458 ChG, EA, EF performed the modelling

459 ASM, CaG, DB, FM, FP, GT, MK, MLM, VG designed and performed the plant experiments

460 NP performed the confocal imaging experiment

461 JL analysed the RNA-seq and genomic data

462 ChG, FP and EA wrote the paper with the help of all authors

463

464 **Competing interests**

465 The authors declare no competing interests.

466

467 **Data and Materials Availability**

468

469 All data are in the main paper or the supplement.

470

471 All plant materials are available upon request.

472 The following secure token has been created to allow review of record GSE150627 while it

473 remains in private status: khkjgckmdtkhpgb.

474 All source codes to run the simulations are available as supplementary archive file (description

475 of installation and execution available as README.txt.

476

477

478 **Supplementary Materials:**

479 Materials and Methods

480 Figures S1 to S6

481 Tables S1 to S3

482 Movies S1 to S3

483 Code archive file: Architecture-model.zip

484 References (41-108)

485 MDAR Reproducibility Checklist

486

487

488